

Electronic Supplementary Information (ESI) for:

Soluble Lanthanide-Transition-Metal Clusters $\text{Ln}_{36}\text{Co}_{12}$ as Effective Molecular Electrocatalysts for water oxidation

Rong Chen,^{#a} Chao-Long Chen,^{#a} Ming-Hao Du,^a Xing Wang,^a Cheng Wang,^a La-Sheng Long,^a
Xiang-Jian Kong,^{*a} and Lan-Sun Zheng^a

^a Collaborative Innovation Center of Chemistry for Energy Materials, State Key Laboratory of Physical Chemistry of Solid Surface and Department of Chemistry, College of Chemistry and Chemical Engineering, Xiamen University, Xiamen 361005, China

[#] These authors contributed equally to this work.

^{*}E-mail: xjkong@xmu.edu.cn

1. Experimental Section:

1.1 Chemicals: Cobalt(II) acetate tetrahydrate ($\text{Co}(\text{Ac})_2 \cdot 4\text{H}_2\text{O}$), Nickel(II) acetate tetrahydrate ($\text{Ni}(\text{Ac})_2 \cdot 4\text{H}_2\text{O}$), Europium nitrate hexahydrate ($\text{Eu}(\text{NO}_3)_3 \cdot 6\text{H}_2\text{O}$), Gadolinium (III) nitrate hexahydrate ($\text{Gd}(\text{NO}_3)_3 \cdot 6\text{H}_2\text{O}$), Dysprosium (III) nitrate hexahydrate ($\text{Dy}(\text{NO}_3)_3 \cdot 6\text{H}_2\text{O}$), Anhydrous alcohol ($\text{CH}_3\text{CH}_2\text{OH}$), Sodium chloride (NaCl), Sodium Carbonate (Na_2CO_3), Sodium hydroxide (NaOH) are analytical grade, and used as received without further purification.

1.2 Sample Preparation.

1.2.1 Synthesis of $\text{Na}_6[\text{Eu}_{36}\text{Co}_{12}(\mu_4\text{-O})_6(\mu_3\text{-OH})_{84}(\text{OAc})_{18}(\text{H}_2\text{O})_{42}(\text{Cl}_2)(\text{NO}_3)_7](\text{NO}_3)_{15}(\text{H}_2\text{O})_{30}$ ($\text{Eu}_{36}\text{Co}_{12}$, **1)** $\text{Co}(\text{Ac})_2 \cdot 4\text{H}_2\text{O}$ (0.245 g, 1.0 mmol) and $\text{Eu}(\text{NO}_3)_3 \cdot 6\text{H}_2\text{O}$ (0.892 g, 2.0 mmol) were dissolved in a mixture of 5 mL deionized water (5.0 mL) and anhydrous alcohol (15.0 mL). Then 10 mg of NaCl and 10 mg Na_2CO_3 were added to the solution. 1.0 mol/L NaOH aqueous solution was added dropwise in the above mixture to the point of incipient but permanent precipitation ($\text{pH} \approx 6$). The mixture was heated to reflux for two hours and then filtered while hot. Block-shaped pink crystals of $\text{Eu}_{36}\text{Co}_{12}$ were obtained in 23.7 % yield (based on $\text{Co}(\text{Ac})_2 \cdot 4\text{H}_2\text{O}$) after the filtrate was kept at room temperature for 1 month. Anal. Calcd. For $\text{C}_{36}\text{H}_{282}\text{Cl}_2\text{N}_{22}\text{O}_{264}\text{Na}_6\text{Co}_{12}\text{Eu}_{36}$ (FW = 11635.38): C, 3.71; H, 2.44; N, 2.65. Found: C, 3.60; H, 2.47; N, 3.06.

1.2.2 Synthesis of $\text{Na}_6[\text{Gd}_{36}\text{Co}_{12}(\mu_4\text{-O})_6(\mu_3\text{-OH})_{84}(\text{OAc})_{18}(\text{H}_2\text{O})_{54}(\text{Cl}_2)(\text{NO}_3)](\text{NO}_3)_{19}\text{Cl}_2 \cdot 20\text{H}_2\text{O}$ ($\text{Gd}_{36}\text{Co}_{12}$, **2)** $\text{Co}(\text{Ac})_2 \cdot 4\text{H}_2\text{O}$ (0.245 g, 1.0 mmol) and $\text{Gd}(\text{NO}_3)_3 \cdot 6\text{H}_2\text{O}$ (0.902 g, 2.0 mmol) were dissolved in a mixture of 5 mL deionized water (5.0 mL) and anhydrous alcohol (15.0 mL). Then 10 mg of NaCl was added to the solution. 1.0 mol/L NaOH aqueous solution was added dropwise in the above mixture to the point of incipient but permanent precipitation ($\text{pH} \approx 6$). The mixture was heated to reflux for two hours and then filtered while hot. Block-shaped pink crystals of **2** were obtained in 25 % yield (based on $\text{Co}(\text{Ac})_2 \cdot 4\text{H}_2\text{O}$) after the filtrate was kept at room temperature for 1 month. Anal. Calcd. For $\text{C}_{36}\text{H}_{286}\text{Cl}_4\text{N}_{20}\text{O}_{260}\text{Na}_6\text{Co}_{12}\text{Gd}_{36}$ (FW = 11808.73): C, 3.66; H, 2.44; N, 2.37. Found: C, 3.60; H, 2.50; N, 2.44.

1.2.3 Synthesis of $\text{Na}_6[\text{Dy}_{36}\text{Co}_{12}(\mu_4\text{-O})_6(\mu_3\text{-OH})_{84}(\text{OAc})_{18}(\text{H}_2\text{O})_{54}(\text{Cl}_2)(\text{NO}_3)](\text{NO}_3)_{19}\text{Cl}_2\cdot 20\text{H}_2\text{O}$ (3**)** Compound **3** was synthesized by the same method except the substitution of $\text{Eu}(\text{NO}_3)_3\cdot 6\text{H}_2\text{O}$ to $\text{Dy}(\text{NO}_3)_3\cdot 6\text{H}_2\text{O}$ (0.913 g, 2.0 mmol). Anal. Calcd. For $\text{C}_{36}\text{H}_{286}\text{Cl}_4\text{N}_{20}\text{O}_{260}\text{Na}_6\text{Co}_{12}\text{Dy}_{36}$ (FW = 11997.73): C, 3.60; H, 2.40; N, 2.33. Found: C, 4.00; H, 2.53; N, 2.35.

1.2.4 Synthesis of $[\text{Eu}_{36}\text{Ni}_{12}(\text{CH}_3\text{COO})_{18}(\mu_3\text{-OH})_{84}(\mu_4\text{-O})_6(\text{H}_2\text{O})_{54}(\text{NO}_3)\text{Cl}_2](\text{NO}_3)_6\text{Cl}_9\cdot 30\text{H}_2\text{O}$ (4**)** $\text{Ni}(\text{Ac})_2\cdot 4\text{H}_2\text{O}$ (0.249 g, 1.0 mmol) and $\text{Eu}(\text{NO}_3)_3\cdot 6\text{H}_2\text{O}$ (0.892 g, 2.0 mmol) were dissolved in a mixture of 5 mL deionized water (5.0 mL) and anhydrous alcohol (15.0 mL). Then 10mg of NaCl and 10 mg Na_2CO_3 was added to the solution. 1.0 mol/L NaOH aqueous solution was added dropwise in the above mixture until to the point of incipient but permanent precipitation ($\text{pH} \approx 6$). The mixture was heated to reflux for two hours and then filtered while hot. Block-shaped green crystals of **4** were obtained in 21.3% yield (based on $\text{Ni}(\text{Ac})_2\cdot 4\text{H}_2\text{O}$) after the filtrate was kept at room temperature for 1 month.

1.2.5 Synthesis of $[\text{Dy}_{36}\text{Ni}_{12}(\text{CH}_3\text{COO})_{18}(\mu_3\text{-OH})_{84}(\mu_4\text{-O})_6(\text{H}_2\text{O})_{54}(\text{NO}_3)\text{Cl}_2](\text{NO}_3)_6\text{Cl}_9\cdot 30\text{H}_2\text{O}$ (5**)** Compound **5** was synthesized by the same method except the substitution of $\text{Eu}(\text{NO}_3)_3\cdot 6\text{H}_2\text{O}$ to $\text{Dy}(\text{NO}_3)_3\cdot 6\text{H}_2\text{O}$ (0.913 g, 2.0 mmol).

1.2.6 Synthesis of $[\text{Gd}_{36}\text{Ni}_{12}(\text{CH}_3\text{COO})_{18}(\mu_3\text{-OH})_{84}(\mu_4\text{-O})_6(\text{H}_2\text{O})_{54}(\text{NO}_3)\text{Cl}_2](\text{NO}_3)_6\text{Cl}_9\cdot 30\text{H}_2\text{O}$ (6**)** Compound **6** was synthesized by reported method (*Angew. Chem. Int. Ed.* **2011**; *50*, 10649).

2. Characterization.

2.1 Measurements. An infrared spectrum was recorded on a Nicolet AVATAR FT-IR360 spectrophotometer with pressed KBr pellets. X-ray photoelectron spectroscopy (XPS) measurements were performed on an ESCALAB 250Xi instrument (Thermo Electron) with Al K α radiation. Inductively coupled plasma-mass spectrometry (ICP-MS) data were obtained with an Agilent 7700x ICP-MS. Thermogravimetric analyses were performed on a Q600 thermal analyzer. Electrospray ionization mass spectra (ESI-MS) were obtained on an Agilent Technologies ESI-MS spectrometer. XAS measurements were carried out at the BL14W1 beamline of the Shanghai

Synchrotron Radiation Facility (SSRF) operated at 3.5 GeV under “top-up” mode with a constant current of 260 mA. Spectra were collected at the europium L₃-edge in transmission mode. The X-ray beam was monochromatized by a Si (111) monochromator and detuned by 50% to reduce the contribution of higher-order harmonics below the level of noise. Three X-ray absorption spectra were collected at room temperature for each sample. Data was processed using the Athena software.

2.2 Single Crystal X-ray Diffraction Determination of single crystals of 1-5. Data of the clusters Data of **1-5** were collected on an Agilent Technologies SuperNova System X-ray single-crystal diffractometer with Cu K α radiation ($\lambda = 1.54184 \text{ \AA}$) at 170 K. Absorption corrections were applied using the multiscan program SADABS.^[1] The structures were solved by direct methods (SHELXTL Version 5.10),^[2] and the non-hydrogen atoms were refined anisotropically by full-matrix least-squares method on F². The hydrogen atoms of organic ligand were generated geometrically (C-H = 0.96 \AA , N-H = 0.90 \AA). Crystal data, as well as details of the data collection and refinement, for the complexes are summarized in Table S1. CCDC number of 2048796-2048800 for clusters contains the supplementary crystallographic data for this paper.

3. Electrochemical methods.

The electrochemical measurements were performed in the cell equipped with three electrodes, working electrode, counter electrode (Pt wire) and reference electrode (Ag/AgCl, saturated KCl, +0.21 V vs. NHE). Cyclic Voltammetry (CV), linear scan voltammetry (LSV), controlled-potential electrolysis (CPE) experiments and differential pulse voltammetry (DPV) were recorded using Electrochemical workstation (CHI 760E, Shanghai Chenhua). For CV, DPV measurement, the 0.07 cm² glassy carbon (GC) electrodes were as the working electrode. For CPE measurements, the clean and dry Indium tin oxide (ITO) glasses served as the working electrodes. All potentials were reported versus normal hydrogen electrode (vs. NHE). Working electrode pretreatment before each measurement included polishing with 0.05 μm alumina paste followed by rinsing with water, and drying in air. All redox potentials in the present work are reported versus NHE by adding 0.21V to the measured potential. CVs were collected at 100mV/s unless otherwise mentioned. No IR compensation was employed. In typical experiments, a stream of argon in atmospheric pressure was

bubbled into the cell for 20 min prior to scanning. The generated O₂ was measured by gas chromatography with a thermal conductive detector with argon as carrier gas (AuLight GC 7920). Faradic efficiency (FE (%)) was calculated based on following equation:

$$FE(\%) = \frac{4 * \text{amount of } O_2 \text{ (moles)} * 100}{n \text{ (moles of electrons)}}$$

$$\text{Where } n = \frac{Q}{F}$$

4. TOF calculation

In Equation (1), the diffusive current i_d was estimated using this couple ($\alpha = 0.5$, $n_d = 2$), A is the area of the electrode, D is the catalyst diffusion coefficient under this conditions. The measured maximum catalytic current i_c varied linearly with the concentration of catalysts, consistent with Equation (2) (the potential for i_c was determined from the DPV). In Equation (2), k_{cat} is the catalytic rate constants, referred as turnover frequency (TOF) of the catalyst, $n_c = 4$ is the number of electrons transferred to generate a mol of O₂. k_{cat} of the catalyst was calculated on the basis of Equation (3).

$$i_d = 0.496 n_d F A [CAT] (\alpha n_d F v D / RT)^{1/2} \quad (1)$$

$$i_c = n_c F A [CAT] (D k_{cat})^{1/2} \quad (2)$$

$$i_c / i_d = 0.323 n_c / \alpha^{1/2} n_d^{3/2} (k_{cat} / v)^{1/2} \quad (3)$$

5. XAS analysis

XAS measurements were carried out at the BL14W1 beamline of the Shanghai Synchrotron Radiation Facility (SSRF) operated at 3.5 GeV under “top-up” mode with a constant current of 260 mA. Spectra were collected at the europium L₃-edge in transmission mode. The X-ray beam was monochromatized by a Si (111) monochromater and detuned by 50% to reduce the contribution of higher-order harmonics below the level of noise. Three X-ray absorption spectra were collected at room temperature for each sample. Data was processed using the Athena software.

Table S1 Single Crystal X-ray Structure Refinement of 1-5.

Complex	Eu₃₆Co₁₂ (1)	Gd₃₆Co₁₂ (2)	Dy₃₆Co₁₂ (3)	Eu₃₆Ni₁₂ (4)	Dy₃₆Ni₁₂ (5)
Formula	C ₃₆ H ₂₈₂ Cl ₂ N ₂₂ O ₂₆₄ Na ₆ Co ₁₂ Eu ₃₆	C ₃₆ H ₂₈₆ Cl ₄ N ₂₀ O ₂₆₀ Na ₆ Co ₁₂ Gd ₃₆	C ₃₆ H ₂₈₆ Cl ₄ N ₂₀ O ₂₆₀ Na ₆ Co ₁₂ Dy ₃₆	C ₃₆ H ₃₀₆ Cl ₁₁ N ₇ O ₂₃₁ Ni ₁₂ Eu ₃₆	C ₃₆ H ₁₀₈ Cl ₁₁ N ₇ O ₂₃₁ Ni ₁₂ Dy ₃₆
Mr	11635.38	11808.73	11997.73	11099.89	11479.33
T(K)	173(2)	173(2)	173(2)	173(2)	123(2)
cryst syst	Orthorhombic	Monoclinic	Monoclinic	Orthorhombic	Monoclinic
space group	<i>Immm</i>	<i>I2/m</i>	<i>I2/m</i>	<i>Immm</i>	<i>C2/m</i>
A, Å	20.8883(9)	20.6147(5)	20.7166(4)	20.8551(3)	28.9037(5)
B, Å	22.4103(9)	28.8773(9)	28.7371(6)	22.5329(4)	28.6333(4)
C, Å	35.1853(13)	22.9058(10)	22.7267(5)	35.0623(5)	20.5500(3)
α/o	90	90	90	90	90
β/o	90	96.475(3)	97.129(2)	90	128.598(2)
γ/o	90	90	90	90	90
V, Å ³	16470.7(11)	13548.8(8)	13425.4(5)	16476.7(4)	13292.0(5)
Z,	2	2	2	2	2
Dc, (g cm ⁻³)	2.346	2.895	2.968	2.237	2.868
μ , (mm ⁻¹)	53.958	63.098	59.763	50.503	55.941
data/params	7161/451	10749/646	10752/792	7492/451	11348/767
θ (deg)	2.32-63.00	2.472-62.00	3.08-65.23	2.46-66.13	2.75-64.97
obsd reflns	23603	22781	39737	23988	38244
$R_1^{[a]}$ [I>2 σ (I)]	0.0743	0.1067	0.0647	0.0939	0.0842
$wR_2^{[b]}$ (all data)	0.2140	0.3092	0.1910	0.2491	0.2441

[a] $R_1 = \sum ||F_o| - |F_c|| / \sum |F_o|$. [b] $wR_2 = \{ \sum [w(F_o^2 - F_c^2)^2] / \sum [w(F_o^2)^2] \}^{1/2}$.

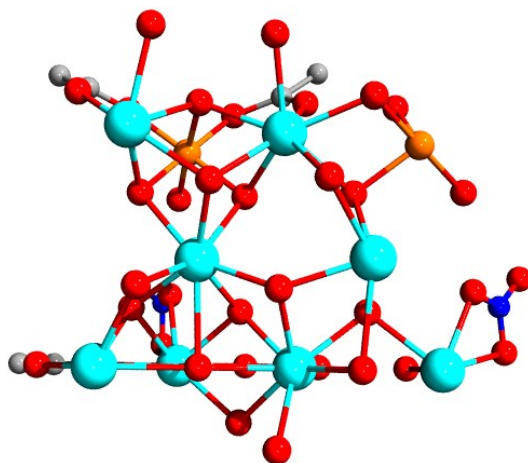


Figure S1. Ball-and-stick plot showing the asymmetric unit of **1**. Ln: turquoise, Co: orange, O: red, C: grey, N: blue. The all H atoms were omitted.

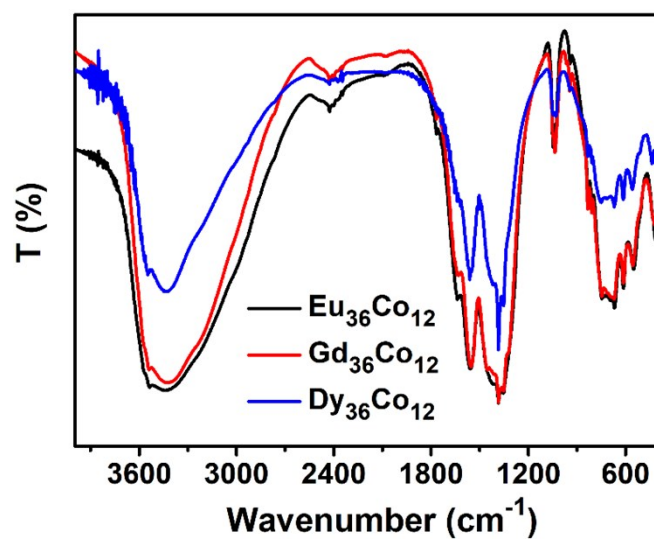


Figure S2. FT-IR spectra in 500-4000 cm^{-1} for $\text{Eu}_{36}\text{Co}_{12}$, $\text{Gd}_{36}\text{Co}_{12}$, $\text{Dy}_{36}\text{Co}_{12}$.

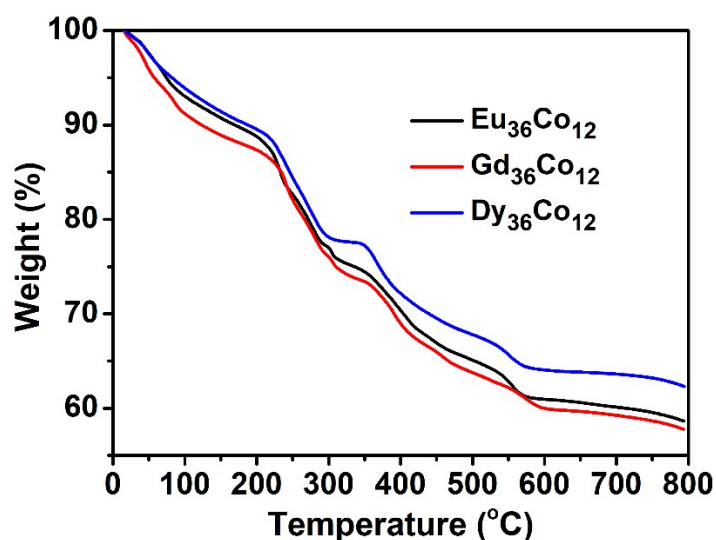


Figure S3. The TGA measurement of $\text{Eu}_{36}\text{Co}_{12}$, $\text{Gd}_{36}\text{Co}_{12}$, $\text{Dy}_{36}\text{Co}_{12}$ under atmosphere. The thermal stability of the clusters was studied by thermogravimetric analysis. According to the thermogravimetric curve, $\text{Eu}_{36}\text{Co}_{12}$ displayed 11.2 % weight loss of the guest and coordination water molecules before 200 $^{\circ}\text{C}$ (Calculated: 11.1 %). From 200 $^{\circ}\text{C}$ to 300 $^{\circ}\text{C}$, the peripheral ligands of $\text{Eu}_{36}\text{Co}_{12}$ began to decompose with 11.3 % weight loss (Calculated: 9.3 %). When the temperature is higher than 300 $^{\circ}\text{C}$, $\text{Eu}_{36}\text{Co}_{12}$ decomposed completely to a mixture of Co_2O_3 and Eu_2O_3 with 58.9 % (observed residues, calculated: 58.3 %). The $\text{Gd}_{36}\text{Co}_{12}$ and $\text{Dy}_{36}\text{Co}_{12}$ show similar TG curves with that of $\text{Eu}_{36}\text{Co}_{12}$.

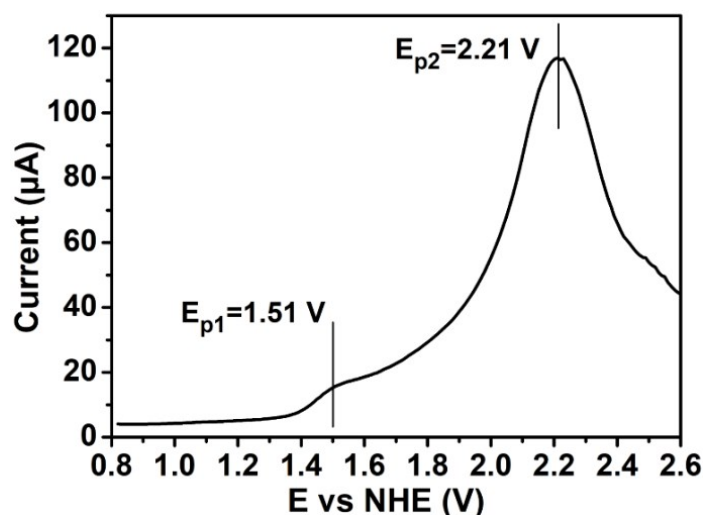


Figure S4. DPV scan for $0.25 \text{ mM } \text{Eu}_{36}\text{Co}_{12}$ in 0.5 M NaAc/HAc buffer solution at $\text{pH} = 5.8$.

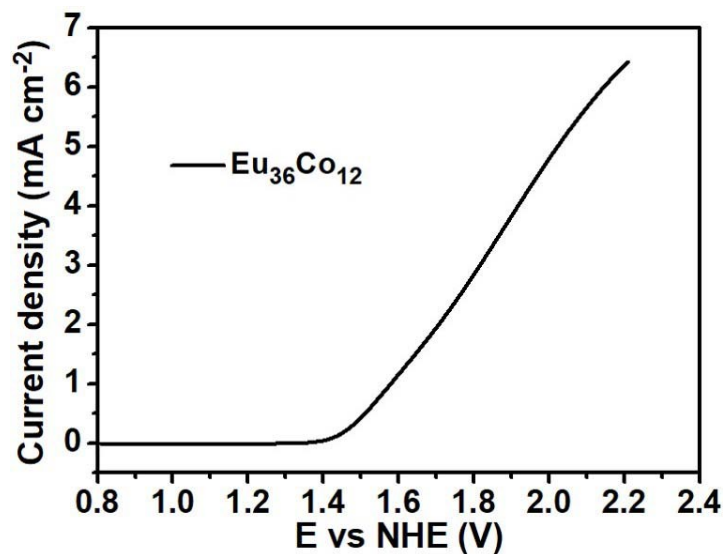


Figure S5. LSV scan before and after 3 hours controlled potential electrolysis (bulk electrolysis) of 0.25 mM $\text{Eu}_{36}\text{Co}_{12}$ in 0.5 M NaAc/HAc buffer solution at pH = 5.8.

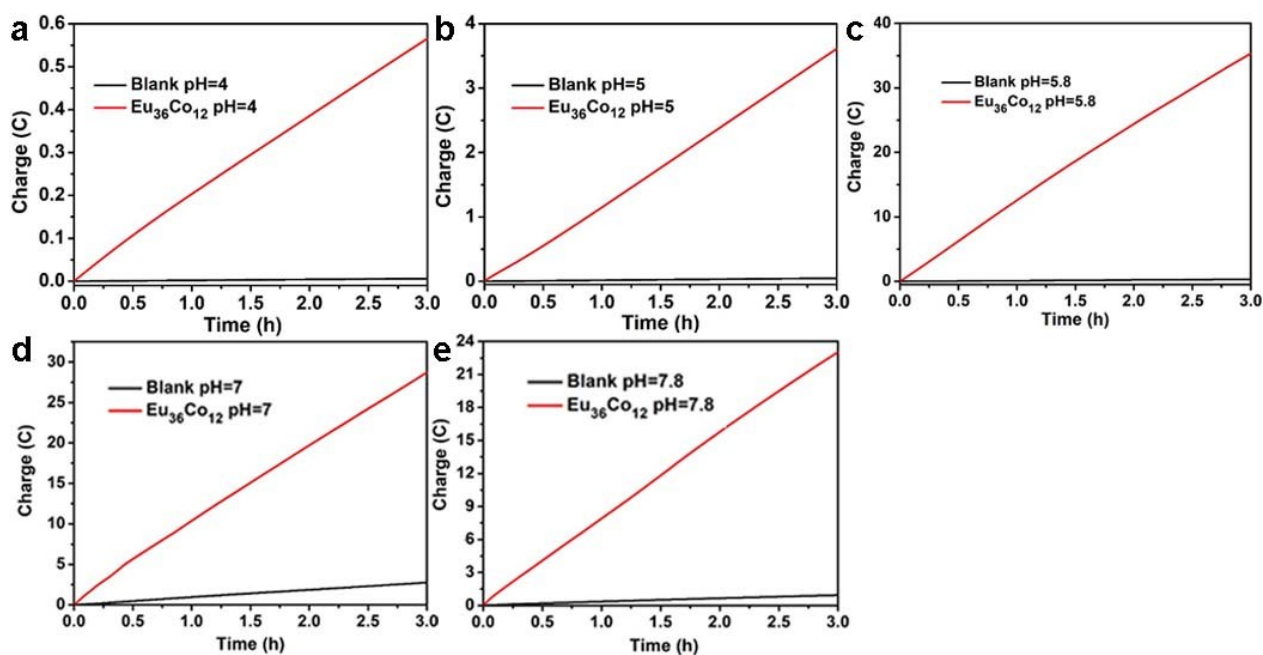


Figure S6. Electrolysis data showing charge passed versus time for a 20 mL solution containing 0.25 mM of $\text{Eu}_{36}\text{Co}_{12}$ in 0.5 M NaAc/HAc buffer solution at different pH = 4, 5, 5.8, 7 and 7.8 (red lines), and data for the buffer solution alone (black lines), with the cell operating at a potential of 1.51 V versus NHE.

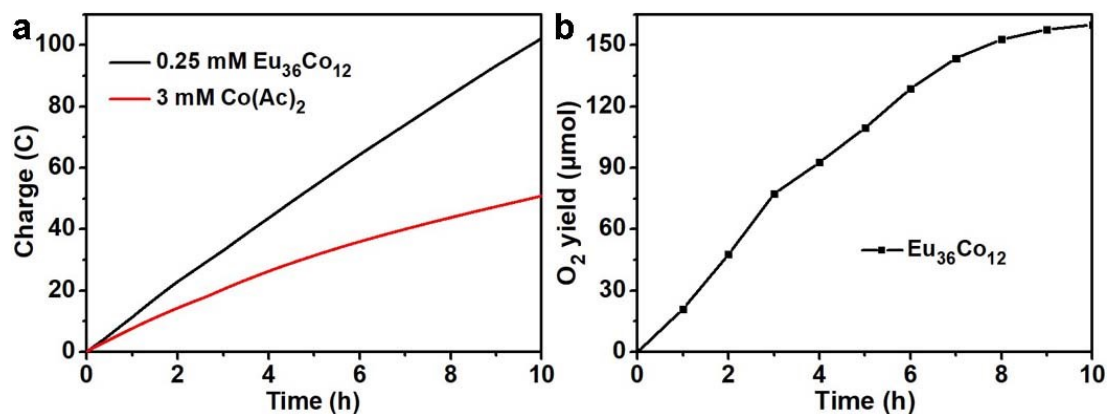


Figure S7. (a) 0.25 mM $\text{Eu}_{36}\text{Co}_{12}$ and 3 mM $\text{Co}(\text{Ac})_2$ of electrolysis data showing charge passed versus time. (b) Oxygen evolution as measured during CPE versus time for 0.25 mM $\text{Eu}_{36}\text{Co}_{12}$.

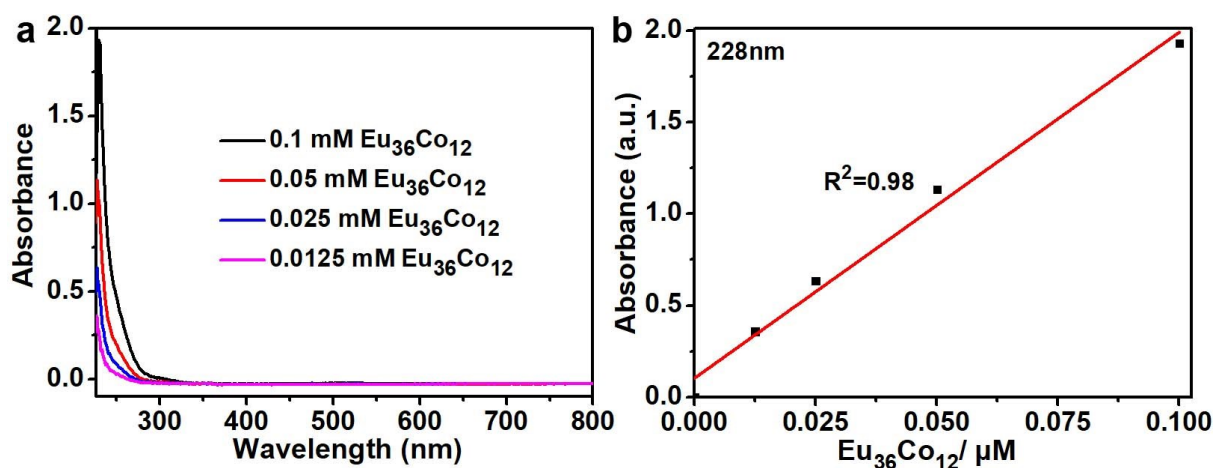


Figure S8. UV-Vis spectra of 0.1 mM, 0.05 mM, 0.025 Mm and 0.125 mM $\text{Eu}_{36}\text{Co}_{12}$ in 0.5 M NaAc/HAc buffer solution (pH = 5.8). (b) The concentration dependence curves of absorbance at 228 nm.

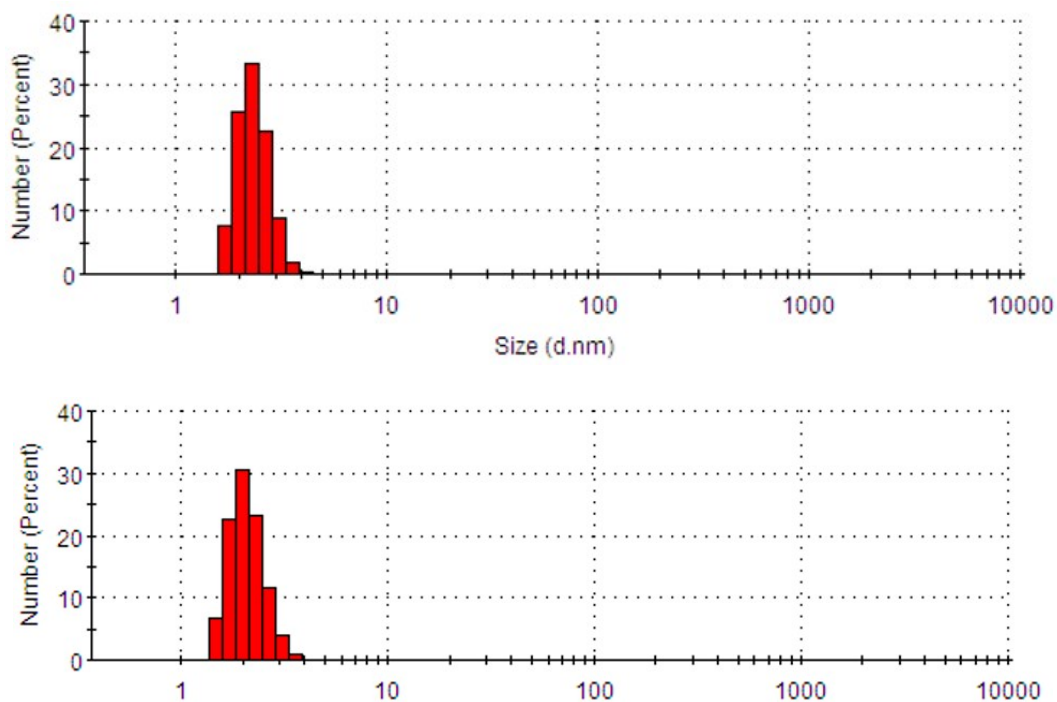


Figure S9. The DLS of $\text{Eu}_{36}\text{Co}_{12}$ at pH = 5.8 and the DLS of $\text{Eu}_{36}\text{Co}_{12}$ at pH = 5.8 after 3 h electrocatalysis.

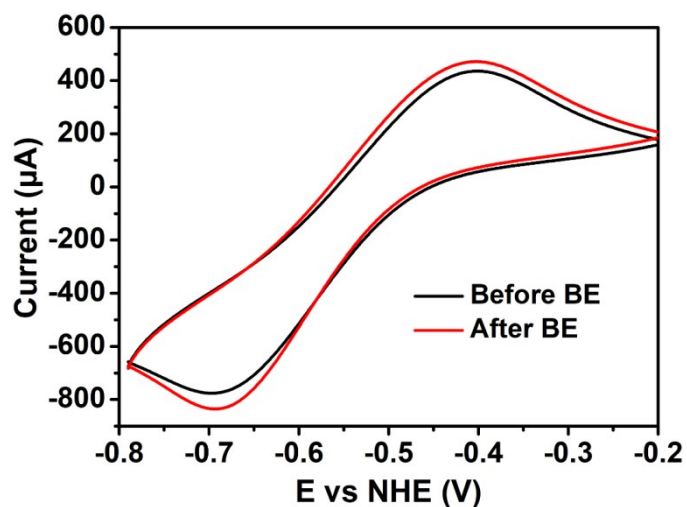


Figure S10. CV scans before and after 3 hours controlled potential electrolysis (BE, bulk electrolysis) of 0.25 mM $\text{Eu}_{36}\text{Co}_{12}$ at pH = 5.8.

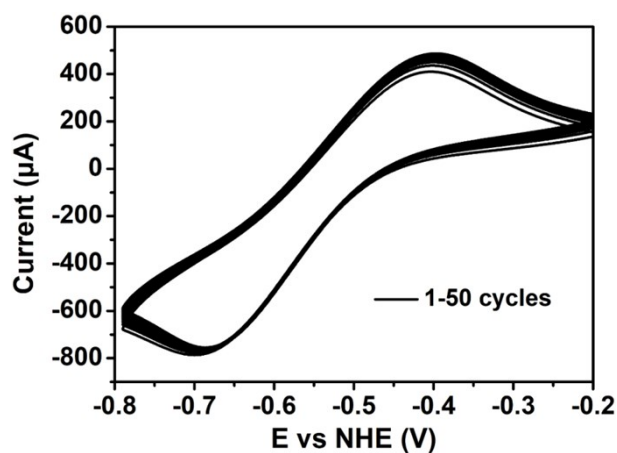


Figure S11. CV scans of $\text{Eu}_{36}\text{Co}_{12}$ over 50 cycles at pH = 5.8.

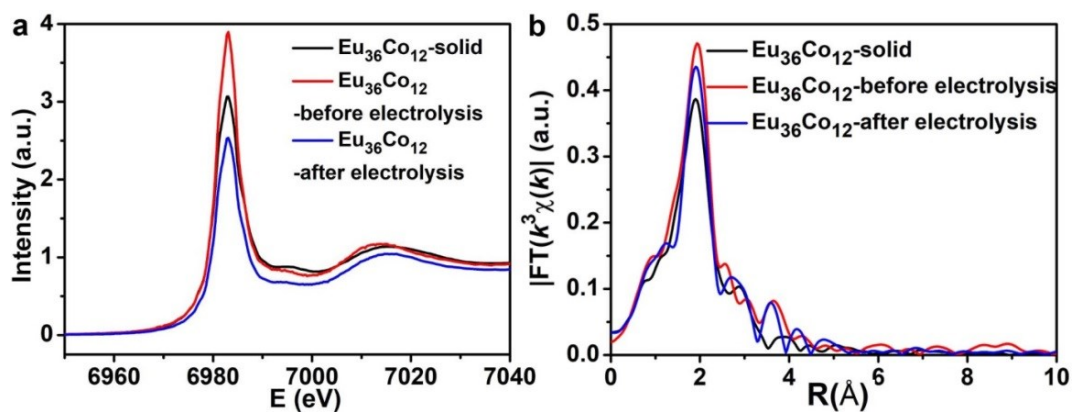


Figure S12. (a) Eu L_3 edge XANES spectra of solid $\text{Eu}_{36}\text{Co}_{12}$, $\text{Eu}_{36}\text{Co}_{12}$ before electrolysis (in 0.5 M pH=5.8 NaAc/HAc buffer solution) and $\text{Eu}_{36}\text{Co}_{12}$ after electrolysis. (b) The corresponding Eu k^3 -weighted FT spectra of solid $\text{Eu}_{36}\text{Co}_{12}$, $\text{Eu}_{36}\text{Co}_{12}$ before electrolysis and $\text{Eu}_{36}\text{Co}_{12}$ after electrolysis.

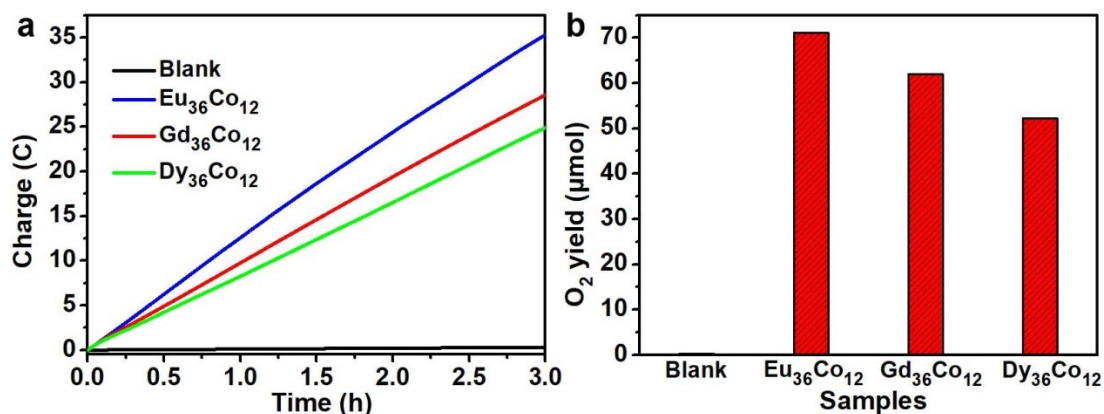


Figure S13. (a) Electrolysis data showing charge passed versus time with blank sample, $\text{Eu}_{36}\text{Co}_{12}$, $\text{Gd}_{36}\text{Co}_{12}$ and $\text{Dy}_{36}\text{Co}_{12}$. (b) Oxygen evolution as measured during CPE versus time for 0.25 mM blank sample, $\text{Eu}_{36}\text{Co}_{12}$, $\text{Gd}_{36}\text{Co}_{12}$ and $\text{Dy}_{36}\text{Co}_{12}$.

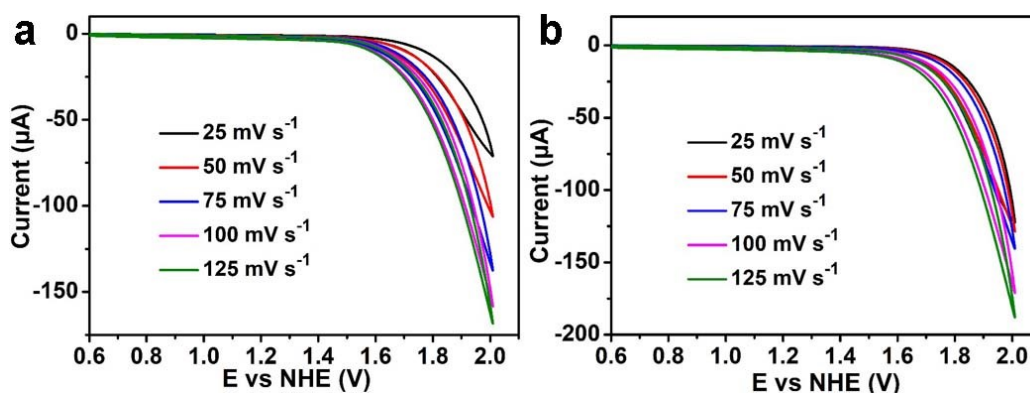


Figure S14. CV of 0.25 mM $\text{Eu}_{36}\text{Ni}_{12}$ at pH 5.8 (a) and 7.8 (b) with different scan rates (25-125 mV s^{-1}) at 0.6-2.0 V.

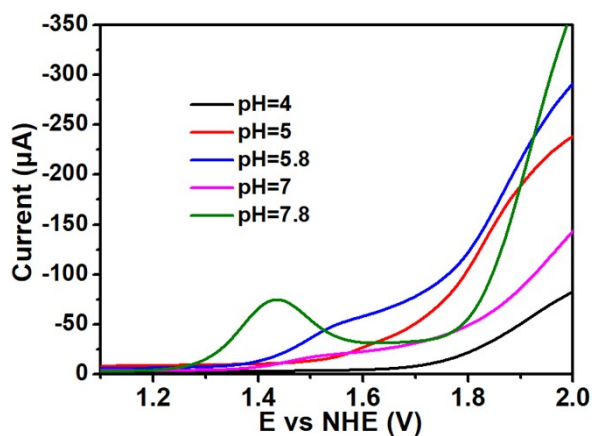


Figure S15. DPV scan for 0.25 mM $\text{Eu}_{36}\text{Co}_{12}$ at pH = 4, 5, 5.8, 7 and 7.8.

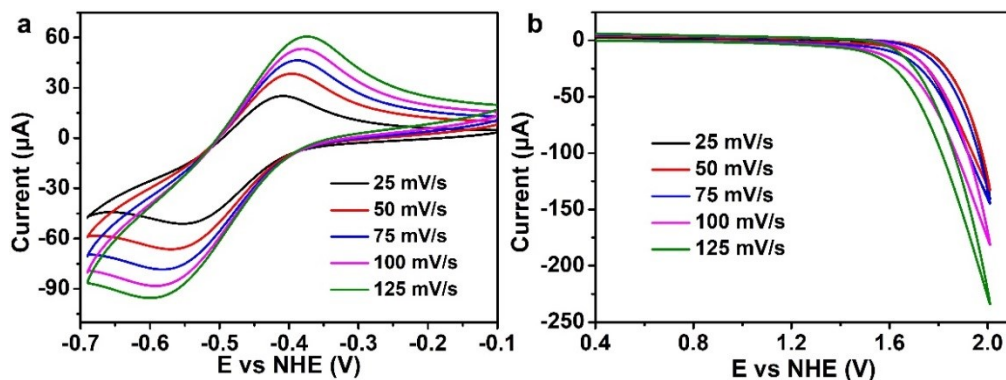


Figure S16. (a) CV of 0.25 mM $\text{Eu}_{36}\text{Co}_{12}$ at pH = 4 with different scan rates (25-125 mV s^{-1}) at (-0.7)-(-0.1) V; (b) at 0.4-2.0 V.

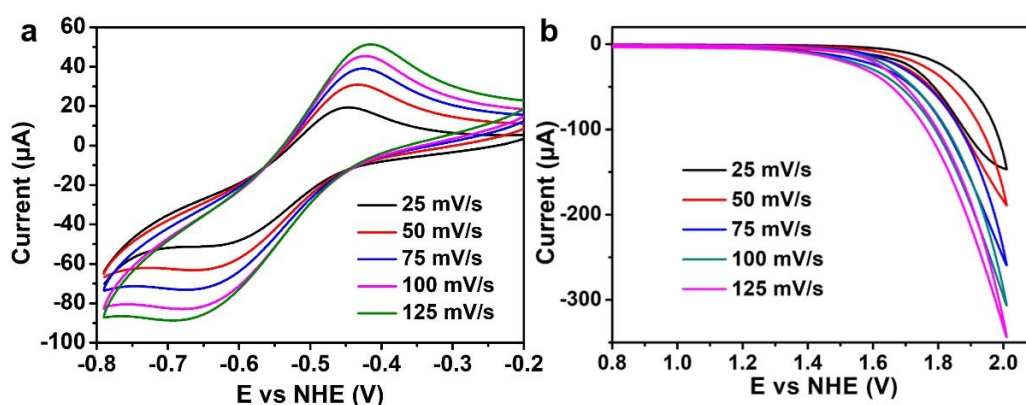


Figure S17. (a) CV of 0.25 mM $\text{Eu}_{36}\text{Co}_{12}$ at pH = 5 with different scan rates (25-125 mV s^{-1}) at (-0.8)-(-0.2) V; (b) at 0.8-2.0 V.

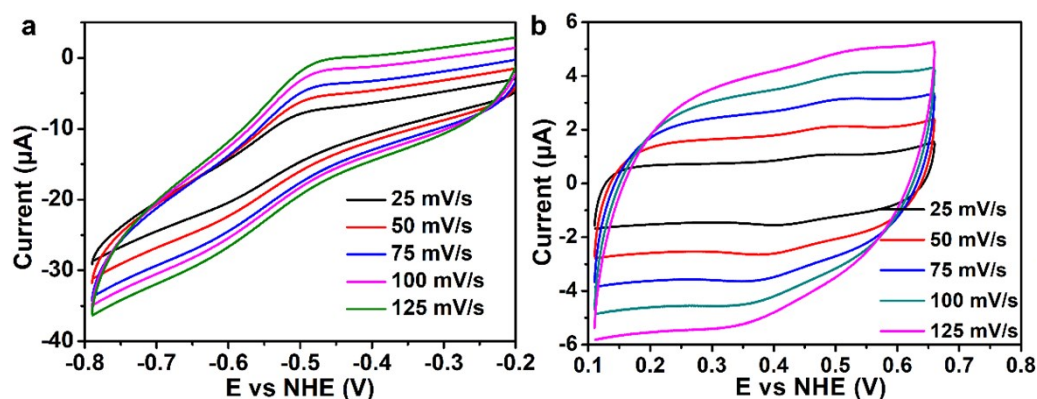


Figure S18. (a) CV of 0.25 mM $\text{Eu}_{36}\text{Co}_{12}$ at pH = 7 with different scan rates (25-125 mV s^{-1}) at (-0.8)-(-0.2) V; (b) at 0.1-0.8 V.

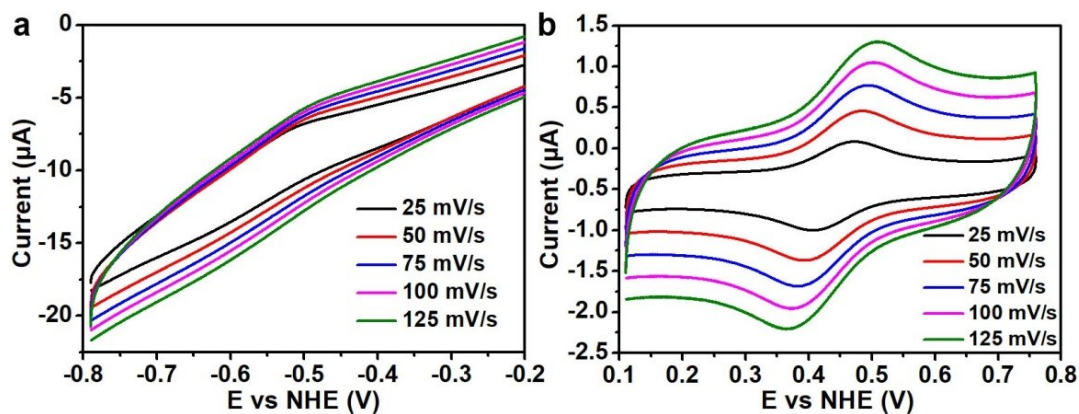


Figure S19. (a) CV of 0.25 mM $\text{Eu}_{36}\text{Co}_{12}$ at pH = 7.8 with different scan rates (25-125 mV s^{-1}) at (-0.8)-(-0.2) V; (b) at 0.1-0.8 V.

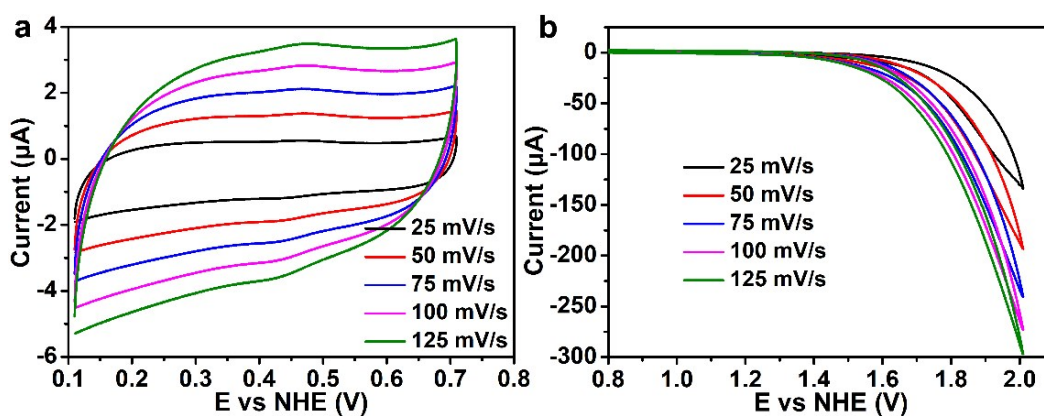


Figure S20. CV of 0.25 mM $\text{Gd}_{36}\text{Co}_{12}$ at pH = 5.8 with different scan rates (25-125 mV s^{-1}) at (a) 0.1-0.8 V; (b) at 0.8-2.0 V.

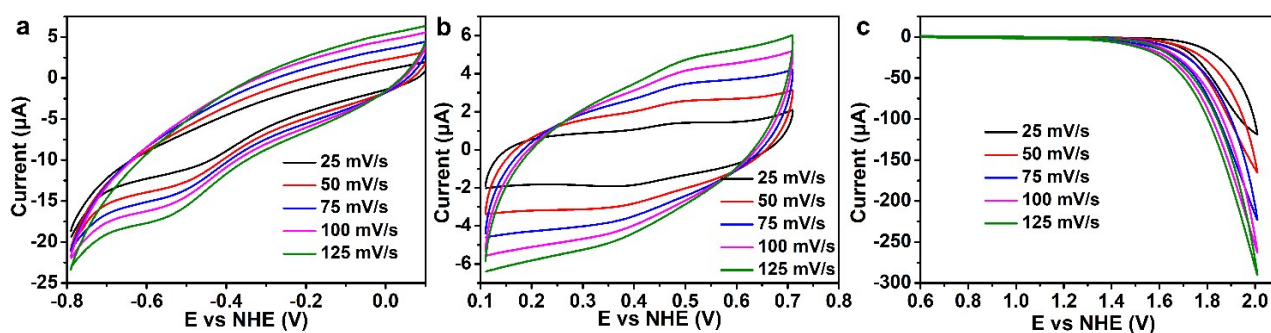


Figure S21. CV of 0.25 mM $\text{Dy}_{36}\text{Co}_{12}$ at pH = 5.8 with different scan rates (25-125 mV s^{-1}) at (a) (-0.8)-(-0.1) V; (b) at 0.1-0.8 V; (c) at 0.6-2.0 V.

Table1. The summary of the catalysts for electrocatalytic water oxidation.

Catalysts	pH	TOF (s ⁻¹)	Overpotential (mV)	Ref.
[Fe ^{II} ₄ Fe ^{III} (μ ₃ -O)(μ-L) ₆] ³⁺	-	1900	>500	1
[(α-SbW ₉ O ₃₃) ₂ Cu ₃ (H ₂ O) ₃] ¹²⁻	7.1	0.7	-	2
[Cu ₄ (pdmH) ₄ (OAc) ₂](NO ₃) ₂ ·3H ₂ O	11.78	0.26	400	3
[Cu ₄ (bpy) ₄ (μ ₂ -OH) ₂ (μ ₃ -OH) ₂ (H ₂ O) ₂] ²⁺	7	-	730	4
[Cu ₂ (TPMAN)(μ-OH)(H ₂ O)] ³⁺	7	0.78	780	5
[Cu(Me ₂ oxpn)Cu(OH) ₂]	10.4	2.14	636	6
Mn ₁₂ DH	6	0.035	334	7
Mn ₁₂ TH	6	22	74	8
[(L _{Gly} -Cu) ₄]	12	267	620	9
[(L _{Glu} -Cu) ₄]	12	105	760	9
Cu ₄ (H ₂ L) ₄ (ClO ₄) ₄	12.5	0.8	500	10
[Co ₉ (H ₂ O) ₆ (OH) ₃ (HPO ₄) ₂ (PW ₉ O ₃₄) ₃] ¹⁶⁻	7	-	353	11
[Cu ₂ (BPMAN)(μ-OH)] ³⁺	7	-	800	12
[Cu ₃ (pda) ₃ (tBuPO ₃)] · 2(Et ₃ NH)	7	0.82	800	13
[Cu ₃ (pda) ₃ (PhPO ₃)] · 2(Et ₃ NH)	-	0.58	-	
[Mn ₄ (H ₂ O) ₂ (PW ₉ O ₃₄) ₂] ¹⁰⁻	7	-	600	14
Cu ₃ L	11	-	620	15
Eu ₃₆ CO ₁₂	5.8	1.5	700	This work

References

- [1] M. Okamura, M. Kondo, R. Kuga, Y. Kurashige, T. Yanai, S. Hayami, V. K. K. Praneeth, M. Yoshida, S. Kawata, M. Shigeyuki. *Nature*, 2016, **530**, 465-468.
- [2] L. Yu, J. Lin, M. Zheng, M. Chen, Y. Ding. *Chem. Commun.*, 2018, 54, 354-357.
- [3] W. S. Gao, J. M. Wang, N. N. Shi, C. N. Chen, Y. Fan, M. Wang. *New J. Chem.*, 2019, **43**, 4640-4647.

- [4] T. T. Lia, Y. Q. Zheng. *Dalton Trans.*, 2016, **45**, 12685-12690.
- [5] Q. Q. Hu, X. J. Su, M. T. Zhang. *Inorg. Chem.*, 2018, **57**, 10481-10484.
- [6] L. L. Zhou, T. Fang, J. P. Cao, Z. H. Zhu, X. T. Su, S. Z. Zhan. *J. Power Sources*, 2015, **273**, 298-304.
- [7] G. Maayan, N. Gluz, G. Christou. *Nat. Catal.*, 2018, **1**, 48-54.
- [8] T. Ghosh, G. Maayan. *Angew. Chem. Int. Ed.*, 2019, **58**, 2785-2790.
- [9] X. Jiang, J. Li, B. Yang, X. Z. Wei, B. W. Dong, Y. Kao, M. Y. Huang, C. H. Tung, L. Z. Wu. *Angew. Chem. Int. Ed.*, 2018, **57**, 7850-7854.
- [10] V. K. K. Praneeth, M. Kondo, P. Woi, M. Okamura, S. Masaoka. *ChemPlusChem*, 2016, **81**, 1123-1128.
- [11] S. Goberna-Ferrón, L. Vigara, J. Soriano-López, J. R. Galán-Mascarós. *Inorg. Chem.*, 2012, **51**, 11707-11715.
- [12] X. J. Su, M. Gao, L. Jiao, R. Z. Liao, P. E. M. Siegbahn, J. P. Cheng, M. T. Zhang. *Angew. Chem. Int. Ed.*, 2015, **54**, 4909-4914.
- [13] J. M. Wang, Y. R. Liu, X. Y. Mao, N. N. Shi, X. Zhang, H. S. Wang, Y. H. Fan, M. Wang. *Chem. Asian J.*, 2019, **14**, 2685-2693.
- [14] S. Goberna-Ferrón, J. Soriano-López, J. R. Galán-Mascarós. *Inorganics*, 2015, **3**, 332-340.
- [15] Ł. Szyrwił, D. Lukács, T. Ishikawa, J. Brasun, Ł. Szczukowski, Z. Szewczuk, B. Setner, J. S. Pap. *Catal. Commun.*, 2019, **122**, 5-9.